LEGS/HRC-S Performance: Linearity Analysis with Mg-K_α Focus Check Data

Stephen S. Murray

18 May 1998

Contents

1 Introduction

This memo responds to the Technical Report by J.J. van Rooijen regarding AXAF Coordinate Systems and Non-Linearities AXAF-LETGS/JJvR/04.05.98

I have carried out an independent analysis of the XRCF data set LHS-FC-1.002 to determine whether there are any unexpected non-linearities or geometrical distortions of the HRC-S, as reported in the above referenced Technical Report. The processing was carried out using the standard HRC data system *HUTDAS* HRC UNIX Tools Data Analysis System (Murray and Chappell), modified to support the larger size of the full HRC-S. When properly analyzed, these data indicate no anomalies or non-linearities in the HRC-S when used as a readout for the LETG.Discontinuities in the HRC-S V-axis coordinate readout (which occur at the segment boundaries) were not taken into account by the SRON analysis (perhaps these are not included in the ASC analysis).

2 Data Processing

2.1 Data Sources

The HRC EGSE data file corresponding to the TRW Test ID LHS-FC-1.002 is s0910430.rd, indicating an HRC-S data file taken on day 091 (at XRCF) beginning at about 04hr 30min GMT. This file was obtained from the standard HRC XRCF data archive. Since this was a test with the FAM operating in dither mode, the corresponding FAM data files were also required. These files were obtained from the ASC XRCF data archive.

2.2 De-gapping

Since the data were taken in the "pre-fix" state of the HRC-S, I used the PHA averaged de-gap maps for each HRC-S segment, derived from Flat Field testing at SAO by Ralph Kraft, as posted on the HRC WWW page (http://hea-www.harvard.edu/HRC/HomePage.html). These de-gap maps are two dimensional tap-by-tap second order polynomial corrections to the raw fine position determination algorithm. It is unlikely that either this detailed de-gap procedure or this most recent de-gap maps were used in the ASC processing system. Thus, the processed data used by the SRON group may be degraded. However, the HRC-S (as well as the HRC-I) is designed so that any de-gapping errors are not cumulative, i.e., the spacing of the taps is set by physical construction of the detectors and the de-gapping only can effect pixels within a tap. Errors in de-gap are usually at the few pixel level regardless of where an event is detected and the difference in processing is most likely not significant.

2.3 De-dithering

The FAM dither correction process used for this analysis consists of determining "good time intervals" (gti) during which the FAM was not moving, and selecting only those HRC events that correspond to these times. For each interval, the photon positions are corrected for the FAM location relative to the zero point of the observation. Such details as the FAM scale factor (0.99937) and FAM axes orientation relative to the HRC-S (10.171 arcminutes) are included in the FAM correction. The only "free" parameter is the relative time offset of the FAM and HRC IRIG clock data. For day 091 this has been determined to be about 10 seconds.

Figure 1 shows the FAM dither pattern during the observation time. The serpentine pattern steps most rapidly in the Y-axis and less rapidly in the Z-axis. The dither extent is about 1mm in Y and 0.3mm in Z. The FAM Y-axis is in the direction of the HRC-S V-axis, and the FAM Z-axis is in the opposite direction of the HRC-S U-axis.(Some independent tests suggest that when in dither mode the FAM requires additional settling time between steps, but this was not considered necessary since the added blur is of order a single HRC pixel, and the loss of data would have been about 50%.) The FAM good time interval file is derived from the FAM readout data that spans the same time as the HRC data.

2.4 Processing Steps

Included for completeness are the series of processing steps used to obtain the data products used for analysis.

```
gunzip -c s0910430.rd.gz | tm2ftm | nftm2prd | nprd2epr > s0910430.nepr
neprs2epr -Fpre_fix -Es0910430.nepr
nepr_sel_fgti -t10 -Gfam_091.fgti -IHRCS <s0910430.nepr >s0910430_fgti.nepr
nepr_sel -u2040 -U2120 <s0910430_fgti.nepr >s0910430_fgti_sel.nepr
```

The de-gap map files are taken from the HRC WWW page (URL http://hea-www.harvard.edu/HRC/prefix/prefixhrcs_qe.html):

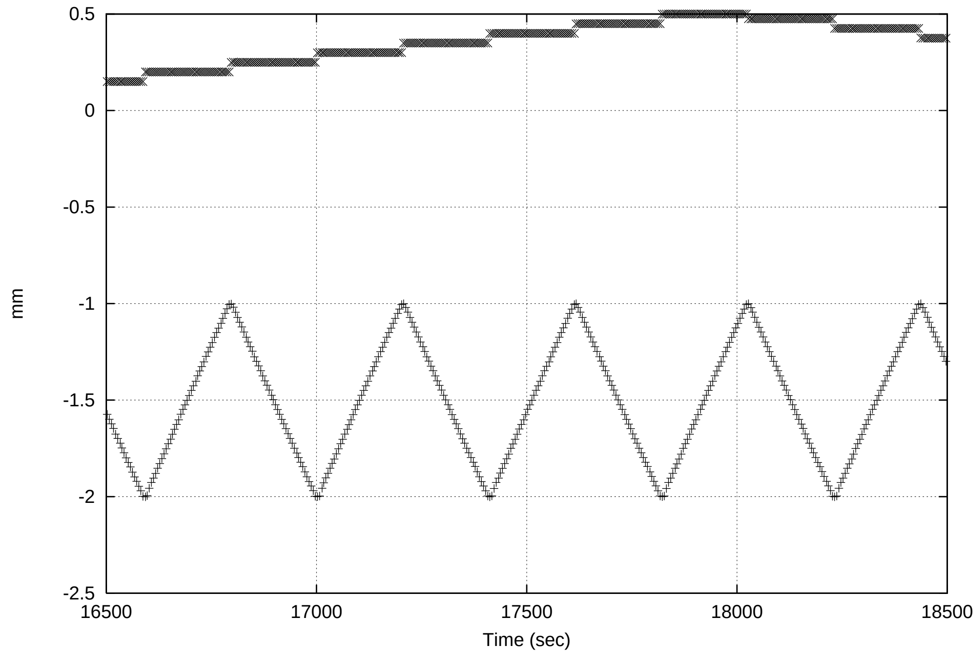

Figure 1: FAM Serpentine dither pattern during the observation

```
pre_fix-1.dgp
pre_fix0.dgp
pre_fix+1.dgp

nfam2spr <fam_091.dat | nspr2fgti > fam_091.fgti
```

3 Data Products

I am interested in determining the locations of the Mg-K_α peak (at about 1.2536 keV) for the various orders that are detected in this test. Thus the strip of data along the dispersion direction was selected for further analysis. The original data file included about 250,000 events. About half of these are rejected as being detected while the FAM indicated it was in motion. Of these good time interval events, about 108,000 were included in the selected strip of data.

3.1 Projected Spectrum

Figure 2: Full image of the HRC-S/LETG measurement for Mg-K.

Figure 2 shows the resulting image of the entire HRC-S. The knife blades were used to block the zeroth and first order images from the detector to avoid over exposure. The gaps between segments are also visible (but since the data are de-dithered, these are slightly washed out). Peaks from the Mg line are seen out to about 15-th order. Using a simple threshold detect algorithm, determining the position centroid, and fitting to a Gaussian profile, the resulting positions for these orders are listed in Table 1. Only the peaks corresponding to the Mg-$K_{\alpha 1}$ line are listed. Beyond the 3-rd order line, the satellite $K_{\alpha 2}$ line is completely resolved and is not confused or blended. For the 3-rd order lines, the peak position is not effected by this satellite line due to the large (x10) intensity difference between the lines. Both the centroid calculation and Gaussian fit positions are listed in the table. It appears that in the cross dispersion direction (U) the peak locations vary systematically with the location along the HRC-S, but more of less symmetrically about the 0-th order. The variation is only 5-10 pixels at the maximum and is not significant with regard to the dispersion direction locations of the peaks.

In Figure 3 an example of the line profile is shown This is the 8-th order line along with a Gaussian fit. The fit gives a line width σ of 8.2 pixels. The separation of the two components is 81.2 pixels, corresponding to about 9.3eV higher energy for the weaker satellite line than the primary line. According to the MIT HETG web site (thanks to Dan Dewey and URL: http://space.mit.edu/HETG/xrcf_sources/sources.html), the Mg Anode yields the Mg-K_α at 1.2356 keV, and two satellite lines at 1.2618 and 1.2632 keV with relative intensity (wrt the main line) of 0.086 and 0.062 respectively. With the LETG/HRC-S combination we are seeing a blend of these satellite lines. Note that at the 8-th order the LETGS resolution (assuming that the primary line width is entirely due to the grating/detector resolution) is 0.0074Å (R=1330)

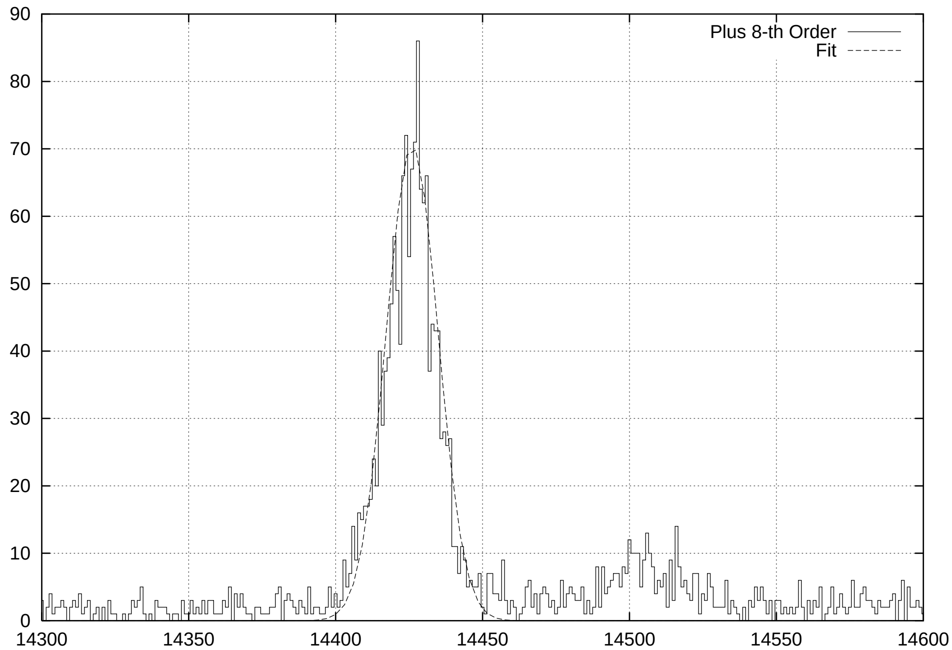

Figure 3: The Minus 8-th order Mg-K_α line complex. The brighter line is at 1.2536 keV, and the dimmer satellite line is at 1.2629 keV. A Gaussian fit to the primary line is plotted, with $\sigma = 8.2$ pixels. The same Gaussian shape is fit to the satellite line, which is clearly resolved in this order (81.2 pixels separate the peaks).

4 Data Analysis

If one assumes a "perfect" spectrometer, then the various orders should be located at spacings given by the relationship:

$$\sin(\theta) = m\lambda/d \tag{1}$$

where m is the order number, λ is the X-ray wavelength (9.890Å), and d is the grating period (9912.16Å).

4.1 Order Spacing

Given the Rowland Circle spacing (RC) for the LETG, the expected locations of the orders on the HRC-S can be calculated. I take the value

$RC = 8788.10mm$ as given in Dan Dewey's HETG WWW page (URL: http://space.mit.edu/HETG/xrcf.html revised 05/08/98). Since the location of the zeroth order is not measured (due to the knife blades blocking the beam) the relevant calculation is the spacing of the orders, which can be compared directly with the measurements.

Using Equation 1 and the value of RC, the spacing of the orders is 1363.9 pixels. (This estimate ignores the small deviations of the HRC-S surface from the Rowland Circle which are no more than about $0.1mm$ at any point along the detector and therefore less than 1 pixel in the location of any feature. The de-gapped coorected pixel scale for HRC-S in the V-axis is 6.4294 $\mu m/pixel$.) Table 1 lists the expected spacing of the orders compared with the measurements and shows that there is an anomalous spacing for the pair of orders that span the transition from the Center segment to the Plus wing. All other spacings are very close to nominal. The mean measured spacing (22 samples) is 1364.3 pixels, to be compared with the expected vale of 1363.9, excellent agreement. The RMS deviation in data sample is 2.6 pixels which is in good agreement with the expected HRC-S performance, the readout alone is characterized by a Gaussian $\sigma = 1.6$ pixels.

The anomalous value for the spacing of orders 6 to 7 is explained by a detailed consideration of the HRC-S construction. This is illustrated in Figure 4 which shows the effect of the 1.4321 degree angle between the center segment and the Plus segment. The HRC-S readout is essentially continuous across the segments; however, the MCPs meet at a height of about 4mm above the readout, at the same angle therefore producing a sudden jump in readout coordinates of about 102.3μm (actually 15.90 pixels). This correction to the spacing gives a value 1369.0 which is consistent with the other measurements.

On the Minus side, the 5-th order line happens to fall on the inter-segment gap and is not detected. The spacing of orders -4 to -6 should be twice the expected value plus the extra spacing due to the tilt of the Minus segment. This jump value is slightly less than for the Plus segment due to the smaller tilt angle (1.2202 degrees), it is about 87.1μm (13.55 pixels). The measured spacing is 2741.8 and the corrected expected value is 2741.4, again in excellent agreement with the observation.

Note that the corrected +6 order value is slightly higher than the expected 1363.9 and may be indictive of a systematic error in the "predicted" value of the discontinuity at the segment boundary. More data sets with

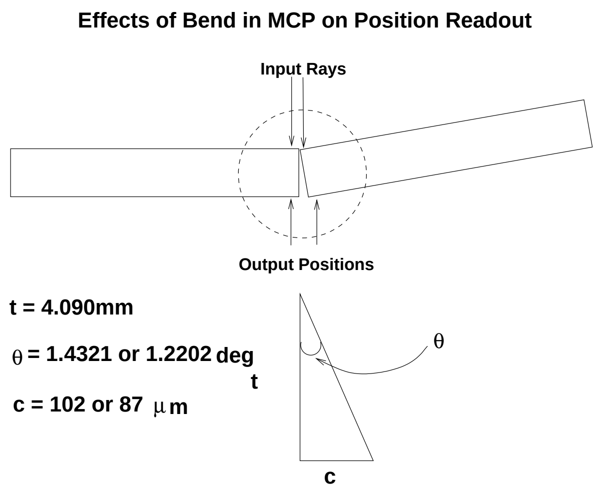

Figure 4: MCPs meet at an angle at their tops and thus are separated at the bottom by the distance 'c' shown in the figure. This distance is a jump in the readout which results in positions which are too large by the corresponding number of pixels.

multiple orders that cross the segment boundaries are needed to examine this effect in a statistically meaningful way. Also other construction effects that might effect the detector performance at the segment boundaries need to be considered. Regardless, there is no evidence within any single segment of any errors regarding the linearity or tilt angle of the segment. Within a segment the order spacings appear to be correct and have no significant systematic trends. The difference betweeen the observed and expected order spacings are shown in Figure 5. For the orders on Segment -1, the mean spacing is 1364.4 ± 2.4, for Segment -0, the means spacing is 1365.5 ± 2.3, and for Segment +1, the mean spacing is 1363.9 ± 3.3.

4.2 Zeroth Order Location

Another analysis of the data can be made by taking the average position of corresponding Plus and Minus orders. The average position should correspond to the location of the zeroth order, and be the same for each pair of higher orders. In Table 1, this analysis is also included. The measured line positions are first corrected for the jumps at each segment, and then the average position for Plus and Minus pairs is calculated. The mean zeroth

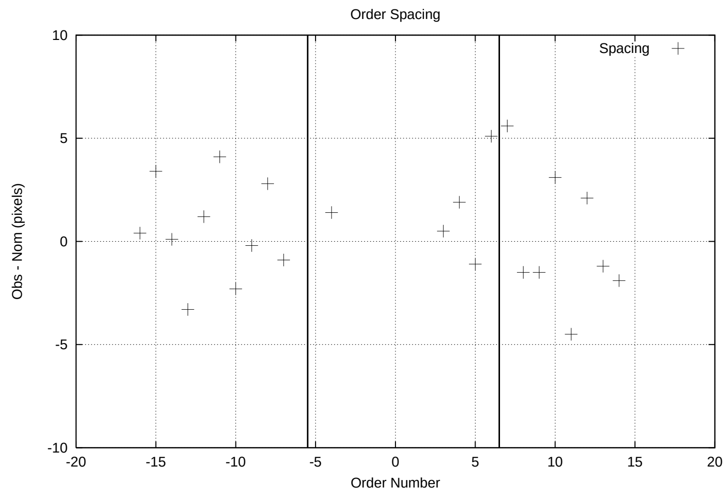

Figure 5: The difference between observed and nominal order spacings versus order. The vertical lines denote the segment boundaries.

order position obtained (in corrected coordinates) is 25344.6 pixels, with an RMS deviation of 1.9 pixels. With these corrections, there appears to be no significant residual systematic errors.

5 Conclusion

The HRC-S performance is excellent with regard to large scale linearity over its entire length. The construction of the detector requires a correction to the calculated v-coordinate which is completely understandable from the geometry of the detector, and can be calculated based on the dimensions of the unit. The precision of these correction terms is slightly uncertain due to some potential assembly variations in the detector from the design values (e.g. the precise thickness of the MCP stack and distance from the CGCD). A similar analysis of additional data could be useful in attempting to model the detector to obtain best fit values for the corrections. However, even at this level of analysis, all of the RMS uncertainties are at the few pixel level.

Table 1: Measured HRC-S v-axis coordinates of the various orders of the Mg-K$-\alpha$ line, and separation of orders. All values in HRC-S pixels (6.4294 μm).

Order	Measured	Separation	Corrected	Center
15	4884.207		4884.2	
14	6246.198	1362.0	6246.2	
13	7608.945	1362.7	7608.9	
12	8974.886	1366.0	8974.9	
11	10334.289	1359.4	10334.3	
10	11701.250	1367.0	11701.3	
9	13063.595	1362.4	13063.6	
8	14425.994	1362.4	14426.0	
7	15795.458	1369.5	15795.5	
6	17180.364	1384.9	17164.5	
5	18543.175	1362.8	18527.3	
4	19908.971	1365.8	19893.1	
3	21273.355	1364.4	21257.5	
-3	29452.237		29436.3	25346.9
-4	30817.452	1365.3	30801.6	25347.4
-5				
-6	33559.298		33529.8	25341.2
-7	34922.269	1363.0	34892.8	25345.2
-8	36289.039	1366.7	36259.5	25342.8
-9	37652.650	1363.7	37623.2	25343.4
-10	39014.256	1361.6	38984.8	25343.1
-11	40382.307	1368.0	40352.8	25343.6
-12	41747.439	1365.1	41717.9	25346.4
-13	43108.003	1360.6	43078.5	25343.7
-14	44471.978	1364.0	44442.5	25344.4
-15	45838.288	1367.3	45808.8	25346.5
-16	47202.588	1364.3	47171.1	